Microgravity Studies in the Liquid-Phase Immiscible System: Aluminum-Indium

S. H. Gelles*
S. H. Gelles Associates, Columbus, Ohio
and
A. J. Markworth†
Battelle Columbus Laboratories, Columbus, Ohio

As part of a study to understand the influence of gravity, cooling rate, and composition on the structure of liquid-phase immiscible materials, two alloys, Al-40 wt% In and Al-70 wt% In, were treated thermally on the SPAR II rocket flight. The treatments involved homogenization at a temperature above the miscibility gap and then rapid cooling through the miscibility gap, followed by complete solidification. The last two steps were performed while acceleration levels were $<4\times10^{-5}$ g. Ground-base reference samples similarly treated showed the expected separation into indium-rich and aluminum-rich layers. The flight alloys, however, produced unexpected results. Instead of fine uniform structures, the alloys consisted of a macroscopically sized aluminum-rich central region surrounded by indium-rich metal. It was reasoned from past results and analyses on configurations formed by gas-liquid mixtures at low g that the structures observed on the flight alloys correspond to those having minimum surface and interfacial energies. Since fluid motion in the microgravity environment is necessary to achieve the final structural configuration, a number of different flow mechanisms were analyzed. Of those analyzed thus far, convection due to density differences, thermocapillary convection, and capillary effects all appear to have a possible role.

I. Introduction

LIQUID-PHASE immiscibles make up a special class of materials, which have gained renewed interest as a result of space-processing activities. These systems contain a so-called miscibility gap, i.e., a field in the binary-phase diagram which represents the equilibrium between two liquids of different compositions. At a sufficiently high temperature, the two-phase equilibrium usually is replaced by a single-phase liquid field. An example of such a system is the aluminium-indium binary-phase diagram presented in Fig. 1.[1,2] The miscibility gap exists above 640°C and between the compositions 17.5 and 96.8 wt% indium. By choosing alloys of composition near the extremities of this range, it should be possible to obtain mixtures of indium droplets in an aluminum-rich host or aluminum-rich droplets in an indium-rich host. A composition near the center of the miscibility gap should yield an intimate mixture of the two phases in about equal proportions or a modulated structure produced by spinodal decomposition.[3] Evidence for spinodal decompositon in liquid systems recently has been presented.[4]

There are many examples of liquid-phase immiscible materials. For example, in a study for NASA, Reger[5] has listed over 500 systems that contain or were suspected of containing a miscibility gap. Some liquid-phase immiscible systems presently are being used in such applications as electrical contacts, permanent magnets, or bearings. There are many other potential applications, for example, in superconductors, superplastic materials, and catalysts. These applications have been explored in recent studies at Battelle's Columbus Laboratories for NASA Marshall Space Flight Center.[6,7]

Presented as Paper 77-122 at the AIAA 15th Aerospace Sciences Meeting, Los Angeles, Calif., Jan. 24-26, 1977; submitted Feb. 22, 1977; revision received Sept. 28, 1977.

Index category: Space Processing.

*Director. Member AIAA.
†Principal Physicist.

The link between liquid-phase immiscibles and space processing evolved from a desire to produce nonsegregated immiscible materials. Although this is an important aspect of the relationship between the two, a more important one was not realized until fairly recently, namely, that, by processing liquid-phase immiscible materials in a low-g environment, not only is the second-phase dispersant expected to be distributed more uniformly, but it also is expected to be much finer.

This conclusion is based on a previous Battelle study,[6,8] in which computer simulation was used to model the agglomeration of liquid droplets in a host liquid. From this study, it was concluded that some major mechanisms causing droplet coalescence are not active at 0 g. These mechanisms depend on gravity-driven collision processes, which result from differences in droplet velocity and are created basically in two ways: 1) Stokes flow, which is the settling or rising of droplets of one density in a host fluid of another density; and 2) gravity-driven convection currents, in which velocity gradients that cause droplet collisions result from gravity-driven convection currents. The latter originate from density differences in the host fluid due to composition or thermal gradients.

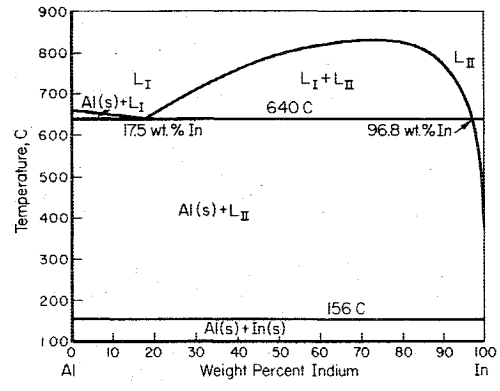

Fig. 1 Aluminum-indium equilibrium diagram.

The finer microstructures anticipated as a result of the computer simulation studies have been observed in liquid-phase immiscibles by Reger and Yates.[9] In addition, some unexpected results have been obtained in the form of unexplained and unidentified phases,[9] unusual electrical properties,[10] and an unusual dependence of the structural fineness on the cooling rate.[11]

This last observation has been made in the bismuth-gallium system after processing in the microgravity environment. In this case, it has been found that a sample that had been cooled slowly exhibited a finer microstructure than one cooled more rapidly. A possible explanation for this behavior has been suggested in terms of convection currents induced by the quenching operation producing droplet collisions and coalescence in the more rapidly cooled sample.

The discovery of unidentified x-ray diffraction lines in gold-germanium and lead-zinc-antimony alloys processed at low g offered the possibility that metastable alloys possessing unusual properties could be obtained in the bulk by space processing. However, a recent attempt to confirm the presence of metastable phases in these alloys has not been successful.[12] This effect therefore must be discounted until further evidence is obtained.

Although our understanding of the coalescence processes in liquid-phase immiscibles has increased significantly in the past two years, we just are beginning the initial stages of a quantitative understanding of the effect of gravity and other system properties on the structures of liquid-phase immiscibles. For example, it is only recently that the first kinetic measurements of droplet size distributions have been obtained in a system with a miscibility gap (aluminum-40 wt% indium alloys cooled through the miscibility gap at two different rates at 1 g[6]). As would be predicted from the computer simulation studies, the population of fine droplets decreased and the concentration of coarse droplets increased as the cooling rate decreased.

The overall objective of this study is to gain an understanding of the influence of gravity, cooling rate, and composition on the structure of liquid-phase immiscible materials. The specific objective of the microgravity experiment (SPAR II experiment 74-30) was to determine the effect of gravity on the structure of the alloys, Al-40 wt% In (13.55 at.% In) and Al-70 wt% In (35.42 at.% In), when cooled through the miscibility gap at a controlled cooling rate (15°C/s). A future rocket experiment originally was planned to study the same alloys processed at a somewhat slower cooling rate. As will be seen in what follows, these plans have been altered at least temporarily pending further analyses of the present experiment.

II. Experimental

The experimental samples were designed to fit into a standard cartridge employed for the general-purpose rocket furnace (GPRF). Experiment 74-30 occupied one of the three chambers in this furnace. The cartridge design is shown in Fig. 2. The pure components for the Al-70 wt% In and Al-40 wt% In alloys were placed in proper proportion in separate aluminum oxide containers, which had been ground carefully to fit the internal dimensions of the stainless-steel capsule. The alloy components have been prepared from high-purity aluminum and indium and have been vacuum-melted individually at approximately 10^{-3} Pa (10^{-5} Torr) to insure that there would be no outgassing during the experiment. Pure components rather than alloys were used in this experiment because greater control of the final alloy composition could be effected in this manner with a system highly prone to macrosegregation.

Final cleaning and adjustment of weights to control the exact composition of the alloy were effected in the case of the aluminum components by etching in a 20 wt% aqueous solution of NaOH and in the case of the indium components by etching in concentrated HCl. In all cases, the compositions were within 0.04% of the composition goal.

An important feature of the cartridge design was the provision for a thermocouple within the Al-40 wt% In alloy (lower alloy in Fig. 2). The thermocouple, ~1 mm o.d., was chromel-alumel sheathed in Inconel and was brazed into the stainless-steel cartridge with a nickel-base alloy. It was protected from the molten metal by an aluminum oxide tube sealed at one end. A stainless-steel tube ~3.2 mm o.d. × 2.2 mm i.d. also was provided at the lower end of the capsule for evacuation and backfilling with inert gas.

After insertion of the assembled crucibles into the stainless-steel capsule, the top end cap was welded in place, whereas the capsule was surrounded with a copper chill designed to prevent melting of the indium components. The cartridges then were leak-checked and were found to be leak-tight within the sensitivity of the helium leak detector used (approximately 4×10^{-10} cm^3/s of helium at STP).

The capsules then were evacuated individually through the tube provided to approximately 3.1×10^{-3} Pa (~3×10^{-5} Torr), backfilled with 0.1 MPa of helium, and re-evacuated to ~2.1×10^{-3} Pa (~2×10^{-5} Torr). This process was repeated twice, and the final backfilling to 1.5×10^{-2} MPa of helium was followed by sealing of the evacuation tube by a resistance spot-welding technique. Leak detection was conducted by placing the entire capsule in a pyrex tube and evacuating the latter with the helium leak detector. No external source of helium was used, and the discovery of leaks depended on detection of helium escaping from the sealed cartridge. No leaks within the sensitivity of the detector were found.

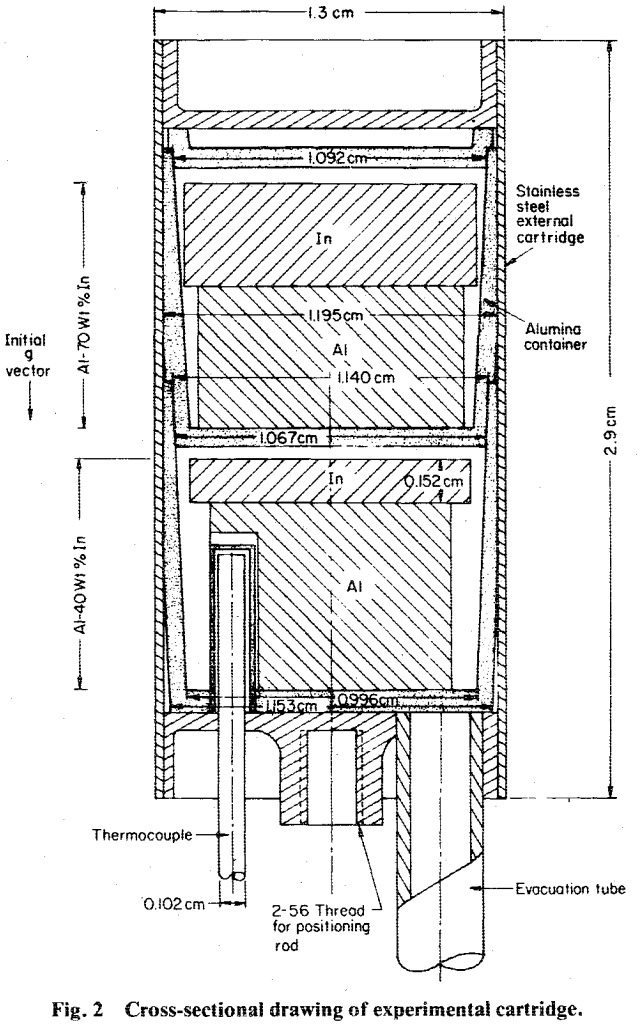

Fig. 2 Cross-sectional drawing of experimental cartridge.

Ground-Base Tests

Several cartridges were subjected to ground-base tests in order to test the capsule design, to determine the proper settings for the general-purpose rocket furnace, to provide the desired heating and cooling conditions, and to produce a reference material with which to compare the micro- and macrostructure of the flight sample. The final ground-base test was carried out on cartridge 74-30-18 in the same orientation as the flight sample. The sample was held for 15 min at 960°C and then quenched with gaseous helium. This procedure resulted in a cooling rate of 17.9°C/s to the monotectic temperature. Since the thermal conditions encountered by cartridge 74-30-18 closely simulated those used in the flight sample, this ground-base sample could be used as a standard with which the flight sample could be compared and was subjected to the same macro- and microstructural analysis as the flight sample.

Flight Parameters

Capsule 74-30-21 was flown in the general-purpose rocket furnace on SPAR II on May 17, 1976. The important flight data are summarized graphically in Fig. 3 and are detailed in Table 1.

The sample was brought to an estimated temperature of 950°C 15 min before launch and held at this temperature through launch and for an additional 154 s into the flight, at which time it was cooled rapidly by means of a helium gas quench. The temperature data telemetered to Earth clearly show evidence of the monotectic transformation, as noted by the plateau on the cooling curve in Fig. 3 and as denoted in Table 1. The average cooling rate from the 950°C hold temperature to the monotectic temperature was 14.7°C/s, close to that of the ground-base reference sample 74-30-18. No thermal effect corresponding to the solidification of indium was noted from the data owing to the slower cooling rate at the lower temperature. However, the indicated temperature fell below 155°C, the equilibrium solidification temperature of indium, at +269 s. It thus is believed that solidification was completed at about this time.

Figure 3 and Table 1 also show that the micro-g level of acceleration ($<4\times10^{-5}$ g) was established 91 s into the flight and continued to ~ +348 s. Cooling of the sample thus began ~63 s after the microgravity level was established, and this level of acceleration lasted approximately 79 s after solidification had been completed.

Another aspect of the flight worth noting is that at launch the rocket was spun about its axis until it reached a maximum spin rate of 240 rpm at +30 s. At +60 s, the rocket was despun rapidly, and approximately 94 s later cooling of the sample commenced. This despinning action and its effect on the molten alloy will be discussed further in a later section of the paper.

An overview of the flight details suggests that, with a minor exception, the flight plan was followed closely. A somewhat lower initial hold temperature (950° vs 970°C) was the only discrepancy noted. This is not considered to be important, since the equilibrium kinetics are expected to be similar for the two temperatures, and since the 950°C temperature is still well above the miscibility gap (see Fig. 1).

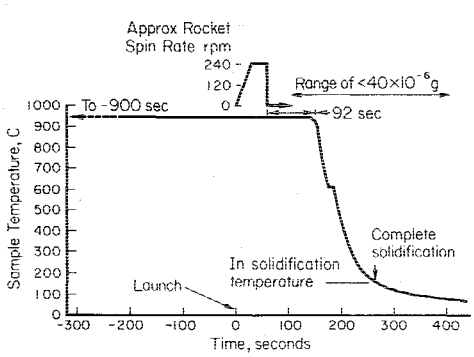

Fig. 3 Thermal history SPAR II experiment 74-30.

Table 1 Thermal history of specimen 74-30-21 and special events in the SPAR II flight

Time, s	Sample temp., °C	Remarks
−900	950 (est.)	Start of preflight temperature soak
−229	949	First temperature data recorded
−200	948	
−150	952	
−100	950	
− 50	954	
− 25	953	
0	954	Launch
+ 25	954	
+ 50	943	
+ 60	...	Rocket despun, maximum acceleration 3×10^{-2} g
+ 75	947	
+ 91	...	Start of low-g period, acceleration <40 μ-g
+100	948	
+125	949	
+150	942	
+154	...	Start of sample cooldown
+176	614	Monotectic arrest
+269	155	Solidification completed
+348	...	End of low-g period, acceleration <40 μ-g

Ground-Base and Flight-Sample Examination

The ground-base and flight samples were examined initially by x radiography and then metallography both on a macro- and microscale. For the metallographic examination, flight and ground-base samples were split longitudinally by means of a SiC water-cooled cutoff wheel approximately 1.25 mm thick. One of the longitudinal samples from each alloy then was polished metallographically and photographed at 4×.

III. Results

The radiographs of the ground-base samples showed a layered structure in both the Al-40 wt% In and Al-70 wt% In alloys, whereas the radiographs of the Al-70 wt% flight sample clearly showed a central lower-density region, roughly spherical in shape, surrounded by a higher-density region. The macroviews shown in Figs. 4 and 5 confirm the radiographic observations. For example, the ground-base alloys (Fig. 5) show the typical layered structures that are expected in terrestrially processed liquid-phase immiscible alloys. The lighter regions at the top of the alloys are aluminum-rich, whereas the darker regions are indium-rich. The relative thickness of the layers is seen to vary in the ex-

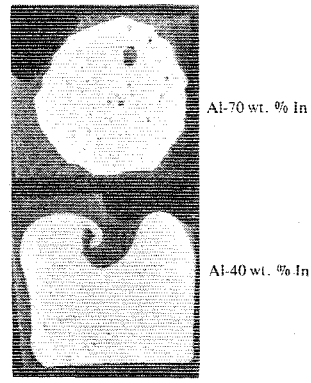

Fig. 4 Macroview of central polished longitudinal section of flight sample 74-30-21 (4× reduced to 60%).

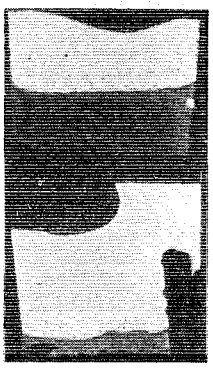

Fig. 5 Macroview of central polished longitudinal section of ground-base sample 74-30-18 (4 × reduced to 60%).

pected way with composition. Careful examination of the macrostructure of the terrestrially processed alloys reveals a relatively high concentration of larger particles in the neighborhood of the layer interface and on both sides of it. As will be shown below, the particles in the aluminum-rich layer correspond to indium-rich droplets that have settled during the cooling process, whereas those in the indium-rich layer correspond to aluminum-rich droplets and dendrites that tend to float in the heavier indium-rich host fluid. It should be noted that there is a great tendency for the indium-rich liquid in the ground-base sample to form a low contact angle with the alumina crucible. This is especially true in the top alloy, Al-70 wt% In, and is visible in Fig. 5, where the indium-rich material has climbed fairly completely up the side of the crucible wall.

The macrostructure of the flight alloys was significantly different from that of the ground-base samples and did not conform to the structure anticipated. Instead of the expected fine, uniform structure composed of indium-rich particles in an aluminum-rich matrix, the Al-40 wt% In alloy (bottom alloy in Fig. 4) was made up of two distinct macroregions, an annular indium-rich layer and an aluminum-rich core. The interface between the aluminum-rich and indium-rich phases shows some wavelike characteristics, especially in the curl form clearly seen in Fig. 4 and previously detected by radiography. The same type of macrostructure also is seen in the Al-70 wt% In alloy (top of Fig. 4). Here the effect is even more dramatic. The central region of the alloy is occupied by an aluminum-rich phase, which takes on a roughly spherical form and again is surrounded completely by an indium-rich layer.

The second-phase particles within the aluminum-rich portions of the flight alloys appear to be fairly uniformly distributed in space but are relatively large in size. The distribution of second-phase particles in the indium-rich regions is not quite as uniform. The aluminum-rich second-phase particles have concentrated in a number of regions, such as the top surface and the interfacial regions near the bottom of both alloys.

The longitudinal sections shown in Figs. 4 and 5 also were examined on a microscopic scale. The photomicrographs of the aluminum-rich region of the Al-70 wt% In alloy, shown in Fig. 6, represent regions at various distances from the interface between the aluminum-rich and indium-rich layers. They clearly show the tendency for the indium-rich particles, which precipitate during cooling through the miscibility gap, to settle out in the Earth's gravitational field. The same effect also has been seen in the aluminum-rich region of the Al-40 wt% In ground-base sample. The particles seen in Fig. 6a probably result largely from the monotectic decomposition of L_1 (see Fig. 1), although some still may correspond to fine droplets precipitated in the miscibility gap.

The indium-rich regions of the Al-70 wt% In and Al-40 wt% In alloys from ground-base sample 74-30-18 again demonstrate the tendency for Stokes migration in the gravity field. For example, in the Al-70 wt% In alloy shown in Fig. 7,

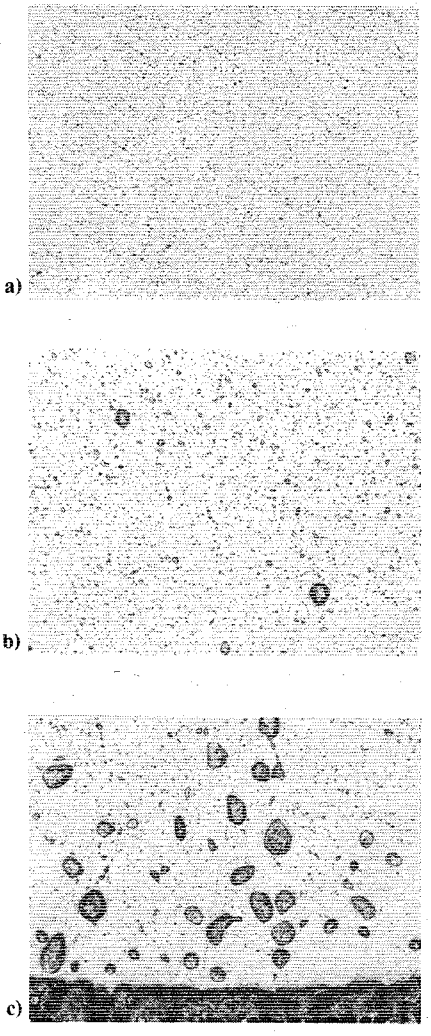

Fig. 6 Photomicrographs of the Al-rich portion of the Al-70 wt% In alloy: ground-base sample 74-30-18. a) 3 mm above interface between Al-rich and In-rich layers, b) 1.5 mm above this interface, and c) at interface (100 × reduced to 60%).

the tendency for aluminum-rich spherical particles that precipitate in the miscibility gap to float upward in the heavier indium-rich liquid clearly is shown. The droplets appear to concentrate in the interfacial region between the aluminum-rich and indium-rich layers. The structure of these spherical particles consists of an outer light-colored (aluminum-rich) layer surrounding a darker (indium-rich) core. This structure presumably results from the monotectic decomposition of the L_1 droplets.

Aluminum-rich dendrites also are present in the indium-rich layers of the ground-base alloys. The dendrites generally are located at a region further displaced from the interface between the layers and often appear to have nucleated at the aluminum-rich portion of the spherical particles. They are thought to arise in a portion of the indium-rich layer which is relatively low in aluminum content and at a temperature below the monotectic temperature.

Two other features of the indium-rich layers present in the ground-base samples are to be noted. First of all, angular particles $\sim 20\ \mu$ in size also are present in the microstructure. They are thought to originate from the SiC cutoff wheel used to section the samples or from the polishing papers. Hard particles from one or both of thse sources become embedded in the soft indium-rich portion of the alloys. Another feature to be noted is the presence of relatively large aluminum-rich spheres along the alloy/aluminum oxide interface (see Fig. 7c). Similar particles also have been seen along cavities

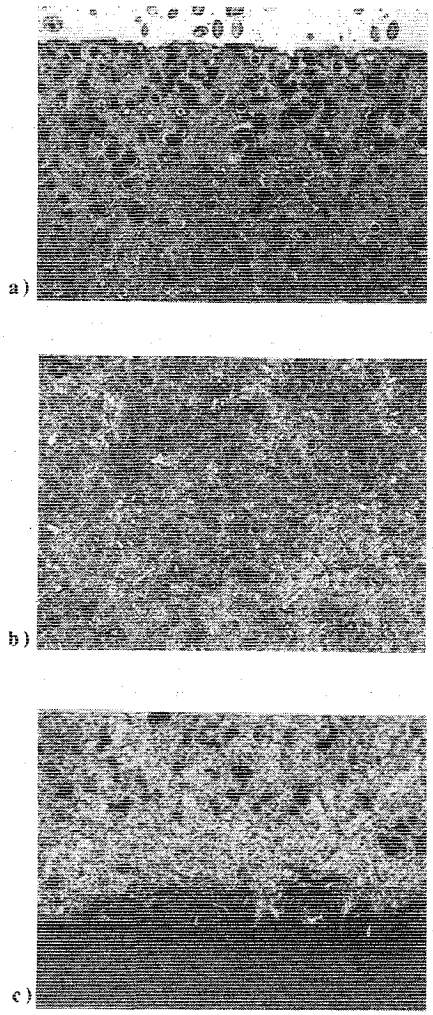

Fig. 7 Photomicrographs of indium-rich portion of the Al-70 wt% In alloy: ground-base sample 74-30-18. a) At interface between Al-rich and In-rich layers, b) displaced 1 mm into In-rich layers, and c) at bottom alumina surface (100× reduced to 60%).

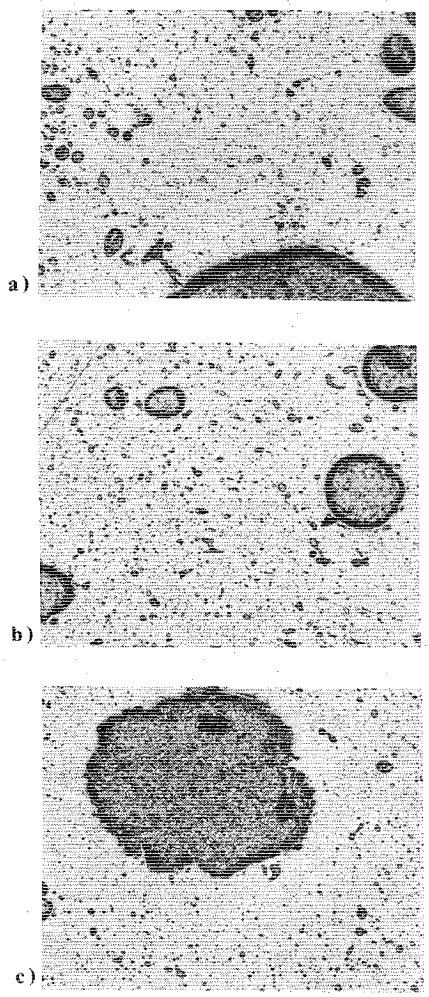

Fig. 8 Photomicrographs of Al-rich portion of Al-70 wt% In alloy: flight sample 74-30-21 (100× reduced to 60%).

(presumably gas bubbles). These interfaces appear to be a source of entrapment for the precipitating aluminum-rich spheres.

In general, the microstructural features of the flight alloys are similar to those in the ground-base samples. However, the second-phase particles generally are distributed more uniformly. The aluminum-rich portions of the Al-70 wt% In and Al-40 wt% In flight alloys show indium-rich particles in an aluminum-rich matrix (see Fig. 8). The larger of these particles are roughly spherical in shape and have formed during cooling through the miscibility gap. However, some of the very large indium-rich particles appear to have aluminum-rich dendrites or spherical droplets precipitated within them (see Fig. 8c). These larger particles have structures that are similar to the bulk indium-rich phase and may, indeed, be part of this phase.

The phases present in the indium-rich portions of the Al-70 wt% In and Al-40 wt% In alloy flight samples are very similar to those in the ground-base sample, but their distribution is much more random and uniform (see Fig. 9). Here, as in the ground-base samples, both aluminum-rich spheres and dendrites are present, but now the dendrites not only nucleate at the spherical particles but also are seen to nucleate at the bulk aluminum-rich phase (see Fig. 9a). Again, larger aluminum-rich spheres appear to be associated with the surface or with the indium/aluminum oxide interface. Also, angular particles attributable to the cutoff wheel or polishing abrasive should be noted and dismissed as an artifact.

IV. Interpretation of Results

General Interpretation

Although the results have not been analyzed completely at this time, it is clear that the behavior of the ground-base samples was close to that expected, whereas that of the flight sample was totally unexpected.

Ground-Base Sample 74-30-18

The evaluation of the Al-40 wt% In alloy ground-base sample is consistent with the following model. The alloy starts out as a homogeneous liquid at 970°C, from which temperature it is cooled rapidly. At ~760°C (see Fig. 1), a fairly large number of indium-rich droplets precipitate and begin settling rapidly, agglomerating and partially forming an indium-rich layer. This process essentially divides the alloy into two alloys, an aluminum-rich one and an indium-rich one. Further cooling leads to precipitation of aluminum-rich, spherically shaped liquid droplets in the indium-rich layer. The aluminum-rich spheres float upward in the heavier indium-rich liquid and concentrate at the region of the interface between the alloy layers. When the alloy reaches the monotectic temperature, ~640°C, the aluminum-rich host fluid in the upper alloy transforms monotectically producing solid aluminum and fine indium liquid droplets. The aluminum-rich liquid droplets in the bottom portion of the alloy also transform and thereby produce particles consisting of a solid aluminum annulus and an indium-rich core. Further cooling of the alloy leads to precipitation of aluminum dendrites in the indium-rich liquid. Finally, at a temperature of ~155°C, the indium solidifies. This description of the

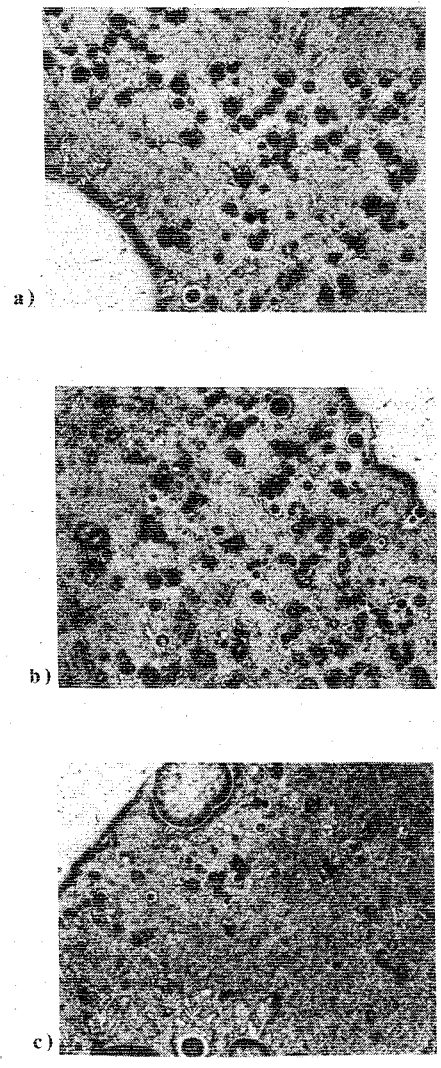

Fig. 9 Photomicrographs of In-rich portion of Al-70 wt% In alloy: flight sample 74-30-21. a) Region B of Fig. 4, b) region A of Fig. 4, and c) region C of Fig. 4 (100× reduced to 60%).

observed microstructure is based on the assumption that mechanical separation by means of Stokes migration at 1 g is a rapid process compared to diffusional processes. This seems reasonable in view of the fact that, within the ~10 s that the alloy is within the miscibility gap, particles ~10 μ can move completely through the alloys.

The same description also could fit the microstructure of the Al-70 wt% In ground-base alloy. In this alloy, however, it is not clear whether indium-rich droplets initially precipitate in an aluminum-rich host fluid, or whether the reverse is true. In either event, the droplets will migrate under the influence of gravity and produce a separation into aluminum- and indium-rich layers. Events subsequent to the layering action should be similar to those delineated for the Al-40 wt% In alloy.

Rocket Flight Samples

The observation of massive segregation in the SPAR II rocket flight sample and the relative coarseness of microstructural features indicate that large fluid flows have occurred at the micro-g acceleration levels encountered in these experiments. Possible causes of this fluid flow are as follows: rocket spin, density differences, thermocapillary forces (Marangoni effect), phase changes, capillary forces, and alloy segregation. A number of these possibilities have been analyzed as detailed below. This work is by no means complete and is presented here as a progress report.

The fluid flow driving forces will tend to produce a mixture of phases having the lowest configurational energy. Some effort has been expended, therefore, at calculating some of the configurational energies.

Effect of Rocket Despin on Fluid Motion

Analysis of residual motion caused by the rapid despin of the rocket from 240 to 0 rpm at +60 s has been treated by Lacy.[15] Lacy has performed terrestrial experiments to determine the effect of viscosity, container geometry, position of the spin axis, and fluid wetting characteristics on the damping time T. The latter was defined as the total time to reach an angular velocity of 0.1 rad/s (corresponding to a tangential velocity of 0.05 cm/s in our case) and was found to vary according to the empirical relationship $T=0.074\, d^2\, \nu^{-1}$, where d is the container diameter and ν is the kinematic viscosity. Lacy also assumed that the velocity decayed exponentially. Hence, for a tangential velocity an order of magnitude slower (0.005 cm/s), the constant of proportionality increases from 0.074 to 0.105. For this latter case, the damping time for the Al-40 wt% In alloy liquid at 1000°C ($\nu=2.8\times10^{-3}$ cm^2/s) in a 1-cm-diam container would be ~38 s. For the liquid Al-70 wt% In alloy under the same conditions ($\nu=1.9\times10^{-3}$ cm^2/s), the damping time would be 55 s. This calculation is based on the published values of the viscosity of pure aluminum and pure indium and assumes that the viscosity of the alloy is a linear function of the atomic percent of indium.

The SPAR II flight sample was allowed a damping period of 94 s between rocket despin and the start of the cooling period (see Table 2). When this time is compared with the calculated damping times, the period appears to be long enough to damp the motion to very small velocities. This is especially true for the Al-40 wt% alloy, in which the presence of a thermocouple should decrease the damping time further.

Thermocapillary Flow (Marangoni Effect)

The fact that the surface tension generally is temperature-dependent implies that temperature gradients existing within a liquid bounded by a free surface may result in convection currents. The Marangoni number Ma, which is a dimensionless quantity, can be used to estimate the relative degree to which this phenomenon can be expected to contribute in a given situation. It is given by $Ma=S(\Delta T)\,d/\alpha\eta$, where S is the temperature coefficient of surface tension, ΔT is the temperature difference existing across the fluid layer, d the depth of the layer, α the thermal diffusivity of the fluid (equal to $K/\rho C$, where K is its thermal conductivity, ρ its density, and C its specific heat), and η the viscosity of the fluid.

Table 2 Calculations of Grashof number and predicted flow velocities at 800°C for $d=1$ cm

Alloy	$\Delta\rho$,[a] g-cm^{-3}	ρ, g-cm^{-3}	ν,[b] cm^2-s^{-1}	Gr at 1 g	Gr at 10^{-5} g	U, cm-s^{-1} at 10^{-5} g
Al-40 wt% In	4.16	3.16	3.26×10^{-3}	1.2×10^{8}	1.2×10^{3}	0.113
Al-70 wt% In	4.16	3.16	2.16×10^{-3}	2.1×10^{8}	2.1×10^{3}	0.098

[a] $\rho_{In}-\rho_{Al}$. [b] Assumes linear relationship with composition expressed in atomic percent.

Let us consider the special case of pure liquid aluminum, taking $\rho = 2.27$ g/cm^3, $C = 0.26$ cal/g-°C, $S = 0.15$ dynes/cm-°C, $\eta = 9 \times 10^{-3}$ P, and $K = 90$ w/m-deg. ΔT was estimated from the rate of heat rejection from the liquid as deduced from the measured cooling rate of ~15°C/s. On this basis, the calculated heat rejection rate of ~4.4 cal/cm^2-s corresponds to an average temperature gradient of ~10°C/cm. Since the distance over which the gradient acts is ~0.5 cm, ΔT should be ~5°C. Insertion of the values of the material parameters into the foregoing equation yields a Marangoni number of 114.

The Marangoni number also has been calculated for the Al-40 wt% In and Al-70 wt% In alloys on the assumption that the only material constants that differ from those of pure liquid aluminum are the densities and viscosities. The calculations resulted in the following values for the Marangoni number at 800°C: *Ma* (Al-40 wt% In) = 229, and *Ma* (Al-70 wt% In) = 500. All of these Marangoni numbers are substantial and would be expected to lead to large fluid velocities. More accurate calculations must await the availablility of accurate values of thermal conductivity, surface tension, viscosity, and density as a function of temperature and alloy composition.

Convection Currents Induced by Density Variations

We have analyzed the extreme condition where density differences as large as $\Delta\rho = \rho_{In} - \rho_{Al}$ might exist in an alloy host fluid of average density, ρ, and might lead to conventional convection.[16] The flow velocity U is governed by the Grashof number *Gr*: $Gr = g\Delta\rho d^3/\rho\nu^2$, where d and ν are defined as before, and g is the acceleration level.

Values of *Gr* calculated for the Al-40 wt% In and Al-70 wt% In are listed in Table 2. Since these values are large, the fluild velocity U can be estimated from $U = \sqrt{Gr}\,\nu/d$.

As may be seen from Table 2, fluid velocities on the order of 0.1 cm/s can result from conventional convection. Since the alloys are in the miscibility gap for approximately 10 s during cooling, flow disturbances on the order of 1 cm might be expected. This very well could contribute to the observed structure.

Bond Number Calculations

The relative importance of surface tension and acceleration forces can be estimated from the Bond number *Bo*, given by $Bo = \rho g d^2/\sigma$, where ρ, g, and d are as defined previously and σ is the surface tension.[13] The Bond numbers for the Al-40 wt% and Al-70 wt % In alloys range between 4.4. and 7.1 at 1-*g* and between 4.4×10^{-5} and 7.1×10^{-5} at 10^{-5} *g* and show that surface tension effects are very important at 10^{-5} *g* and of some importance at 1 *g*.

Equilibrium Configurations

In order to obtain some insight into the most stable geometric configurations for a mixture of aluminum and indium, the sum of the surface and interfacial energies has been calculated as a function of the volume fraction of aluminum for the simple case where there is no container. Three configurations, each 1 cm^3 total volume, have been considered, all in spherical form: 1) an indium annulus surrounding an aluminum sphere; 2) an aluminum annulus surrounding an indium sphere; and 3) two spheres, one aluminum and one indium. The sum of the surface and interfacial energies as a function of the volume fraction of aluminum V_{Al} for the three configurations are as follows:

Al surrounding In

$$4\pi(\tfrac{3}{4}\pi)^{\frac{1}{3}}\gamma_{Al} + 4\pi(\tfrac{3}{4}\pi\{1 - V_{Al}\})^{\frac{1}{3}}\gamma_{Al\text{-}In}$$

In surrounding Al

$$4\pi(\tfrac{3}{4}\pi)^{\frac{1}{3}}\gamma_{In} + 4\pi(\tfrac{3}{4}\pi V_{Al})^{\frac{1}{3}}\gamma_{Al\text{-}In}$$

Separate spheres

$$4\pi(\tfrac{3}{4}\pi V_{Al})^{\frac{1}{3}}\gamma_{Al} + 4\pi\{\tfrac{3}{4}\pi(1 - V_{Al})\}^{\frac{1}{3}}\gamma_{In}$$

where γ_{Al}, γ_{In}, and $\gamma_{Al\text{-}In}$ are, respectively, the surface energies of aluminum and indium and the interfacial energy of the Al-In boundary.

The calculations were performed for an assumed temperature of 800°C, where the surface energy of pure aluminum γ_{Al} is 850 ergs/cm^2 and γ_{In} is 490 ergs/cm^2. The value of the interfacial energy between liquid aluminum and liquid indium, $\gamma_{Al\text{-}In}$, is unknown. If its value is similar to those in other comparable liquid-phase immiscible systems, it should be ~100 ergs/cm^2 or less.[17]

The sum of the surface and interfacial energies is plotted in Fig. 10 as a function of V_{Al} for the three configurations and for two assumed levels of interfacial energy, $\gamma_{Al\text{-}In}$, 200 and 500 ergs/cm^2. The curves of Fig. 10 show that the lowest energy configuration should be the one with the indium annulus surrounding an aluminum sphere over all values of V_{Al} if $\gamma_{Al\text{-}In} < \sim 360$. If $\gamma_{Al\text{-}In} = 500$ ergs/cm^2, the indium-surrounding-aluminim configuration is stable up to a volume fraction of aluminum $V_{Al} = 0.72$. For aluminum contents higher than this value, a configuration consisting of separate aluminum and indium spheres has the lowest surface energy of the three possibilities considered.

In light of the foregoing discussion, it is not surprising that the configuration with indium surrounding aluminum is approximately the one observed in the Löhberg and Ahlborn SPAR II experiment,[18] as well as in the present experiments. Since in the former experiment there was a nonwetting condition between metal and container, the experimental conditions more closely met the assumptions of our calculations. Similar configurations have been encountered in drop-tower samples of the alloy Al-68.8 wt% In.[6,19] These samples were of much smaller diameter (4.2 mm diam × 1.4 cm long) and were processed in graphite containers under nonwetting conditions. Again there was a clear tendency for the indium-rich metal to surround an aluminum-rich core.

The tendency for one of the materials to surround the remainder of the alloy also has been noted in Pb-Zn alloys processed on ASTP[20] and terrestrially in the Bi-Se system.[21] Although it is not clear whether the conditions were wetting or nonwetting, in both cases the material with the lower surface energy surrounded the higher-surface-energy portions of the alloy.[17]

The conditions encountered in the present experiment in which the alloy wets the crucible are much more complicated than the nonwetting situation since two liquids, a gas and a solid, are involved. This situation has not been analyzed as yet, but some insight can be gained from analyses and experiments reported in the literature dealing with contained gas-liquid mixtures at low *g*.[13,14] In thse cases, the configurations depend on the shape of the container, the amount of liquid, and the degree to which the liquid wets the con-

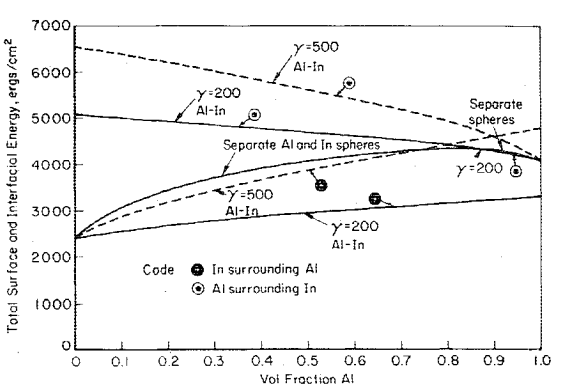

Fig. 10 Total surface energy for various aluminum and indium configurations.

tainer. However, if there is complete wetting, the liquid most often will surround the gas phase. We feel that the configuration observed in the flight sample probably can be explained in a similar way. In the present experiment, the indium-rich liquid wets the alumina crucible (i.e., forms a low-energy interface) and thus tends to surround the aluminum-rich liquid.

In summary, it is possible to produce the observed configuration in which indium-rich metal surrounds an aluminum-rich core in both nonwetting and wetting situations. In the former case, this results from the lower surface energy of the indium-rich liquid relative to the aluminum-rich liquid and the low interfacial energy between them, and in the latter case it results from the relatively low energy of the indium-rich liquid/alumina boundary.

Capillary Effects

Liquid droplet spreading on a solid surface is a possible mechanism by which the indium-rich layer is formed at the container walls from a dispersion of droplets. We just have started to analyze this problem and have determined that spreading of 1 μ droplets is extremely rapid (10^{-7} s) when there is no constraining fluid around the droplet. Somewhat slower spreading times are anticipated when surrounding fluid is present. The spreading action can cause local fluid flow, which may bring other droplets in contact with the solid wall or liquid film, and so further coalescence may proceed by this action.

A somewhat related case involves the rearrangement of the fluid phase in contained gas-liquid mixtures when gravitational forces are largely eliminated. The capillary-dominated motion in these cases depends on the size of the container, but even for relatively large containers (10 cm) the time involved is ~1 s and decreases for smaller containers.[13]

It thus appears that the time scale for such flows is consistent with the present experiment and that capillary flows may be a very important mechanism leading to the observed configurations. Further analysis clearly is required.

V. Conclusions

On the basis of the analysis carried out to date, the following conclusions can be made:

1) Results from processing Al-40 wt% In and Al-70 wt % In samples terrestrially are qualitatively in agreement with those anticipated; a model to explain the macro- and microstructure of the ground-base samples has been presented.

2) The processing of the rocket flight sample proceeded according to plan except for a somewhat lower initial hold temperature.

3) The type of macrostructure resulting from processing the Al-40 wt% and Al-70 wt% In samples in space was unexpected. The morphological evolution can be interpreted in terms of fluid flow occurring in the microgravity environment.

4) Fluid flow in the microgravity region can arise from numerous sources. Of the sources analyzed, thermocapillary convection and conventional convection are probably active; capillary flow as yet has not been analyzed but probably is important. Residual fluid motion due to rocket spin does not appear to make an important contribution.

5) The equilibrium configuration of the aluminum and indium in the microgravity environment has been calculated on the basis of known surface energies of the components and assumed values of the interfacial energy based on those of similar systems. A configuration of an annular ring of indium surrounding an aluminum-rich core is predicted and agrees closely with the observations in the present system, as well as with some past results.

6) Bond number calculations support the observation that surface tension forces in this alloy system are dominant in the microgravity environment.

Acknowledgments

The authors appreciate the helpful interaction and discussions with R. Chassay, I. C. Yates, L. L. Lacy, F. Reeves, and B. Aldrich of NASA Marshall Space Flight Center. They also appreciate the helpful discussions with S. Ostrach of Case-Western Reserve University, R. Brodkey of Ohio State University, and T. Cochran of NASA Lewis Research Center. They also wish to thank A. Webster for his painstaking efforts in assembly of the ground-base and flight capsules. This research was conducted at Battelle Columbus Laboratories and was sponsored by NASA under Contract NAS8-31543.

References

[1] Gelles, S. H., unpublished data, April 1977.

[2] Predel, B., "Beitrag Zur Konstitution und Thermodynamik Von Entmischungssystemen," *Zeitschrift fur Metallkunde*, Vol. 56, No. 11, 1965, p. 791.

[3] Cahn, J. W., "Spinodal Decomposition," *Transactions of the Metallurgical Society of AIME*, Vol. 242, Feb. 1968, p. 166.

[4] Schwartz, A. J., Huang, J. S., and Goldburg, W. I., "Spinodal Decomposition in a Binary Liquid Mixture Near Critical Point," *Journal of Chemical Physics*, Vol. 62, No. 5, 1975, p. 1847.

[5] Reger, J. L., "Study of Processing Immiscible Materials at Zero-G," Interim Rept. to NASA Marshall Space Flight Center, Contract NAS8-28267, May 1973.

[6] Markworth, A. J., Oldfield, W., Duga, J., and Gelles, S. H., "Investigation of Immiscible Systems and Potential Applications," Final Rept. to NASA Marshall Space Flight Center, Contract NAS8-29748, April 1975.

[7] Gelles, S. H., Collings, E. W., Abbott, W. H., and Maringer, R. E., "Analytical Study of Space Processing of Immiscible Materials for Superconductors and Electrical Contacts," Final Rept. to NASA Marshall Space Flight Center, Contract NAS8-31445, Sept. 1976.

[8] Markworth, A. J., Gelles, S. H., Duga, J. J., and Oldfield, W., "Immiscible Materials and Alloys," *Proceedings of Third Space Processing Symposium*, NASA Rept. 74-5, June 1974, p. 1003.

[9] Reger, J. L. and Yates, I. C. Jr., "Preparation and Metallurgical Properties of Low Gravity Processed Immiscible Materials," AIAA Paper 74-207, Washington, D.C., Jan. 30-Feb. 1, 1974.

[10] Lacy, L. L. and Otto, G. H., "The Electrical Properties of Zero-Gravity Processed Immiscibles," AIAA Paper 74-208, Washington, D.C., Jan. 30-Feb. 1, 1974.

[11] Reger, J. L., "Experimental Development of Processes to Produce Homogenized Alloys of Immiscible Metals," Final Rept. to NASA Marshall Space Flight Center, Contract NAS8-27805, Dec. 1972.

[12] Anderson, W. T., "Post Skylab Investigations, Experiment M-557, Immiscible Metal Alloys," Supplemental Rept. to NASA Contract NAS8-28309, Nov. 1975.

[13] Otto, E. W., "Static and Dynamic Behavior of the Liquid-Vapor Interface During Weightlessness," *Aerospace Chemical Engineering*, Vol. 62, No. 61, 1966, p. 158.

[14] Neu, J. T. and Good, R. J., "Equilibrium Behavior of Fluids in Containers at Zero Gravity," *AIAA Journal*, Vol. 1, 1963, p. 814.

[15] Lacy, L. L., personal communication, July 1976.

[16] Ostrach, S., "Convection Phenomena at Reduced Gravity of Importance for Materials Processing," *19th Plenary Meeting, COSPAR*, Philadelphia, Pa., June 18-19, 1976.

[17] Murr, L. E., *Interfacial Phenomena in Metals and Alloys*, Addison-Wesley, Reading, Mass., 1975, pp. 101-106.

[18] Löhberg, K. and Ahlborn, H., "Preliminary Report on the Results of the SOLUOG-Experiment SPAR II: Solidification Behavior of Aluminum-Indium Alloys Under Zero Gravity Conditions," Report to Deutsche Forschungs-und Versuchsanstalt für Luft-und Raumfahrt e. v., July 1976.

[19] Gelles, S. H. and Markworth, A. J., "Rocket Experiment 74-30: Agglomeration in Immiscible Liquids at Low-G," Monthly Progress Rept. to NASA Marshall Space Flight Center, Contract NAS8-31543, Aug. 18, 1976.

[20] Ang, C. Y. and Lacy, L. L., "Monotectic and Syntectic Alloys, Experiment MA-044," Apollo-Soyuz Test Project Preliminary Science Rept., NASA Doc. TMX-58173, Feb. 1976.

[21] Knight, R. J., Li, C. Y., and Spencer, C. W., "Monotectic Reaction in the Bi-Se System," *Transactions of the Metallurgical Society of AIME*, Vol. 227, Feb. 1963, pp. 18-22.